PHYSICS OF PLASMAS **19**, 056102 (2012)

Enhanced superbanana transport caused by chaotic scattering across an asymmetric separatrix[a)]

Daniel H. E. Dubin[b)], A. A. Kabantsev, and C. F. Driscoll
Department of Physics, University of California at San Diego, La Jolla, California 92093, USA

(Received 5 December 2011; accepted 31 January 2012; published online 21 March 2012)

This paper discusses a novel "chaotic" form of superbanana transport and compares the theory to experiments on non-neutral plasmas. Superbanana transport is caused by particles that cross local trapping separatrices (magnetic or electric ripples) in the presence of field "errors" such as toroidal magnetic curvature. Traditionally, collisions (at rate ν) cause separatrix crossings, with resulting transport that scales as $\nu^{1/2}B^{-1/2}$. The "chaotic" transport of interest here occurs when the separatrix is "ruffled" in the direction of plasma drift; then, collision*less* particle orbits give random trapping and detrapping. Prior theory assumed a "stellarator symmetry" and suggested that these orbits give reduced transport scaling as ν^p with $p \sim 1$. Here, we fully characterize chaotic transport and show that the transport is enhanced rather than reduced, scaling as $\nu^0 B^{-1}$. Experiments on pure electron plasmas provide quantitative transport measurements, with precise control of the overall field error, and of the trapping separatrix with and without ruffles. The experiments show close agreement with theory over a decade in B, for both collisional neoclassical transport, and for the distinctive chaotic transport. At low magnetic fields, transport scaling as B^{-p} with $p \gtrsim 2$ becomes dominant, showing preliminary agreement with bounce-resonant theory.
[http://dx.doi.org/10.1063/1.3694053]

I. INTRODUCTION

This paper discusses theory of superbanana transport and compares to measurements in cylindrical pure electron plasmas. The measured transport agrees with superbanana theory in the $\sqrt{\nu}$ regime, and the ν^1 regime[1] only if a certain "stellarator symmetry"[2] is preserved. However, when this symmetry is broken (and in some cases even when it is not) the transport is enhanced, and a novel ν^0 regime occurs, caused by chaotic scattering of trapped particles across asymmetric separatices. As far as we know, this is the first quantitative comparison of experiment to superbanana transport theory.

In order to understand how stellarator transport can be modeled in the much simpler cylindrical geometry of a Penning-Malmberg trap, we note that the major ingredients of superbanana transport are

1. A global "field error" that causes particles to drift off of flux surfaces. This is the toroidal curvature of the magnetic field in stellarators and is a controlled tilt of the magnetic field in our experiments.
2. Separate populations of locally trapped and untrapped particles which experience different drifts. This is caused by magnetic field ripples in stellarators; and by a controlled electric potential barrier in our experiments.
3. A separatrix between trapped and untrapped particles which varies with poloidal angle around the flux surface. In stellarators, the magnetic field ripples vary with poloidal angle, so particles encounter different barrier heights as they drift around the surface; in our experiments, the electric potential has controlled azimuthal variations termed "ruffles" (to distinguish these asymmetries from the global error field).

Thus, all three superbanana transport features occur in the cylindrical pure electron plasma, shown schematically in Fig. 1. The plasma is confined for hundreds of seconds in a quiescent, stable equilibrium, without the turbulent transport that occurs in neutral plasmas. The magnetic field is tilted by a small angle $\epsilon_B \equiv B_\perp/B_z \lesssim 10^{-3}$ radian in a chosen direction $\theta_B \equiv \tan^{-1} B_y/B_x$, creating the global field error which causes the dominant radial particle transport. The "squeeze" voltage $V_{\rm sq}(\theta)$ applied to the central electrode creates a trapping barrier $\phi_{\rm sq}(r,\theta) = qV_{\rm sq}(r,\theta)$, shown with a $\cos(2\theta)$ ruffle. Control of the barrier allows us to distinguish between the various types of neoclassical transport.

II. BOUNCE-AVERAGED TRANSPORT THEORY

Single particle orbits in these fields are shown schematically in Fig. 2. Cyclotron dynamics is assumed to be at sufficiently high frequency so that it can be entirely neglected. Particles with parallel energies E above $\phi_{\rm sq}$ bounce from end to end of the plasma, with a bounce frequency $\omega_b(E)$. Particles with parallel energies less than $\phi_{\rm sq}$ are trapped on one or the other side of the squeeze barrier. All the particles perform $\mathbf{E} \times \mathbf{B}$ drifts in the magnetic field, which in the bounce-averaged drift approximation are roughly circular orbits with bounce-averaged frequency $\omega_E(E)$. Because of the tilt in the field (assumed to be a vertical tilt in the figure) these circular orbits are shifted vertically; particles trapped on the right side of the squeeze have orbits shifted upwards by an amount Δr compared to passing orbits that average out the tilt field; particles trapped on the left are shifted downward by this

---

[a)] Paper CI2 3, Bull. Am. Phys. Soc. **56**, 56 (2011).
[b)] Invited speaker.

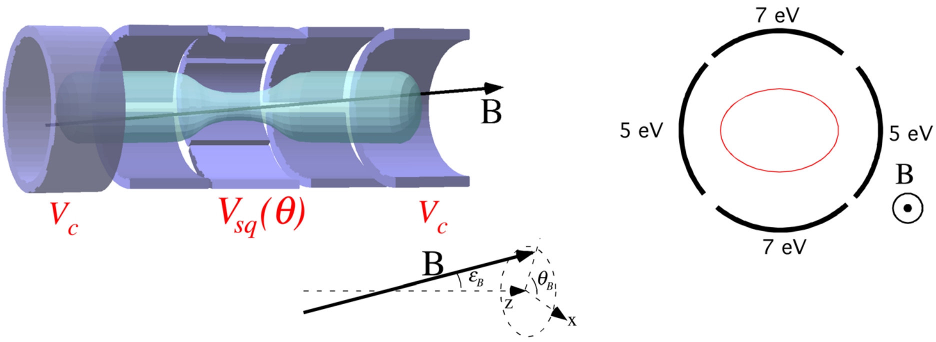

FIG. 1. (Color online) Cutaway view of trapped non-neutral plasma used in superbanana transport studies. The plasma is confined by applying voltages V_c to end electrodes. The magnetic field is tilted by an angle ϵ_B with respect to the z axis of symmetry, and the tilt is oriented in the x-y plane at an angle θ_B with respect to the x axis. A squeeze voltage $V_{\rm sq}(\theta)$ is applied to a central sectored electrode, shown end on in the second view.

amount. The shift is roughly proportional to the tilt angle ϵ_B as well as to the plasma length L_p.

Superbanana transport occurs when the bounce-averaged drift orbits randomly change from passing to trapped and back to passing. These random separatrix crossings can be caused either by collisions or by the chaotic nature of some orbits near the separatrix energy.

The standard superbanana transport regimes arise when collisions at frequency ν are considered to be the separatrix-crossing mechanism. When $\omega_E < \nu < \omega_b$, the transport is in the $1/\nu$ regime.[1,3] Collisions cause particles to change from trapped to passing and back at a rate of ν, as the particle parallel energy randomly diffuses above and below $\phi_{\rm sq}$. In the time $1/\nu$ between trapping and de-trapping, particles complete only a small fraction of their drift orbit, so they step radially by only a small fraction of Δr, approximately $\Delta r \omega_E/\nu$. Since particles are randomly trapped on either the right or left sides of the squeeze, these steps are random in direction and cause radial diffusion D_r at a rate

$$D_r \sim f\nu(\Delta r \omega_E/\nu)^2 \propto \nu^{-1}B^{-2}, \tag{1}$$

where f is the fraction of trapped particles. However, this $1/\nu$ regime requires large collisionality and so has not been observed in current experiments, because the experiments always have $\nu < \omega_E$.

A second regime, which has been probed experimentally, occurs when $\nu < \omega_E < \omega_b$; this is the $\sqrt{\nu}$ regime.[1,4,5] In this regime, transport is due to particles in a collisional boundary layer that occurs around the separatrix energy $\phi_{\rm sq}$. The boundary layer is caused by the difference in the orbits of trapped and passing particles. This induces a discontinuity in the collisionless distribution function across the separatrix, which is smoothed out by collisions. The width of the collisional boundary layer ΔW_c is[6,7]

$$\Delta W_c = \sqrt{T\phi_{\rm sq}\nu/\omega_E}. \tag{2}$$

Particles in this layer are driven by collisional parallel energy diffusion back and forth across the separatrix every rotation period. As the particles are trapped randomly on either side of the squeeze potential, they take random steps of size Δr, producing radial diffusion

$$D_r \sim \omega_E(\Delta r)^2 \Delta W_c/T \propto \nu^{1/2}B^{-1/2}, \tag{3}$$

where the factor $\Delta W_c/T$ is roughly the fraction of particles in the collisional boundary layer.

When the separatrix is ruffled in θ, this transport can be either reduced or enhanced. A θ-variation in separatrix energy $\phi_{\rm sq}$ by amount $\Delta\phi$ allows particles with parallel energy in this range around the separatrix energy to *collisionlessly* change from trapped to passing and back as the orbits drift in θ. As these particles are retrapped randomly each rotation period in the right or left trapping wells, radial diffusion results scaling as

$$D_r \sim \omega_E(\Delta r)^2 \Delta\phi/T \propto \nu^0 B^{-1}. \tag{4}$$

One can see that this result supercedes the previous $\sqrt{\nu}$ regime result when the separatrix ruffle $\Delta\phi$ is larger than the collisional boundary layer width ΔW_c.

III. SYMMETRY CONSIDERATIONS

However, there is an extra complication associated with a certain type of "stellarator symmetry."[2] It is sometimes possible to choose an orientation for the field errors such that particles that collisionlessly change from trapped to passing and back always do so on the same flux surface (radius). A cylindrical example is shown in Figs. 3(a) and 3(b). The tilt

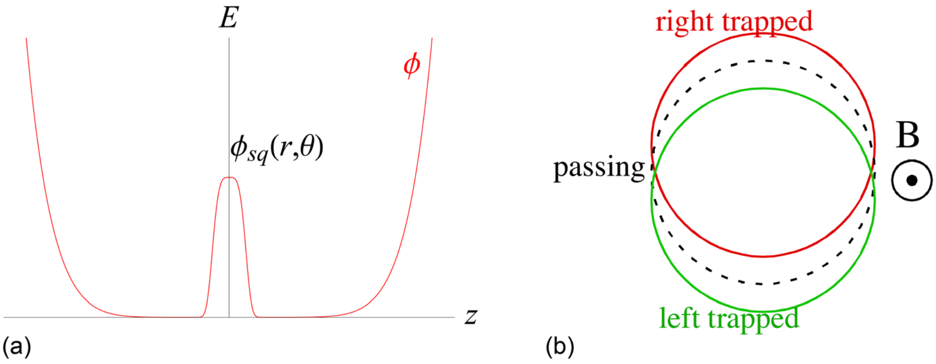

FIG. 2. (Color online) (a) Sketch of the potential in the trap. Particles with energy below $\phi_{\rm sq}(r,\theta)$ are trapped. (b) Bounce-averaged drift orbits in a vertically tilted magnetic field. The green orbit is for a particle trapped in the left well and is shifted down compared to red orbit, which is trapped in the right well, as well as the passing orbit, shown by the dashed line.

of the magnetic field is chosen to be in the vertical direction, and the $m=2$ separatrix ruffle is also chosen to have reflection symmetry along this vertical axis, as shown in Fig. 1. In this symmetric case, denoted $\alpha = 0$, trapped and passing particle orbits are closed, (provided that the ruffle mode number m is less than 3),[9] so $\Delta r = 0$, and no transport results from the collisionless mechanism described previously. Moreover, when collisions are added, the radial diffusion is no longer identically zero, but it is *reduced* compared to the $\sqrt{\nu}$ regime, scaling as

$$D_r \sim \nu^p B^0 \quad (\text{symmetric case}), \tag{5}$$

where the exponent $p \sim 1$.[5,8,9] [Reference 9 finds that $p=1$ for ruffle mode number $m=1$, and $p \sim 11/12$ for $m=2$.] This is the previously mentioned ν^1 regime predicted by standard stellarator superbanana transport theory. Previous work on superbanana transport often assumes this symmetry, but here we consider the more general case.

In our experiments, the symmetry is easily broken by orienting the direction of the magnetic tilt at an angle θ_B which differs from the orientation angle of the ruffle θ_m, giving $\alpha \equiv \theta_B - \theta_m \neq 0$, as shown in Figs. 3(c) and 3(d). Now the drift orbits, which are shifted circles along the direction of the tilt field $\mathbf{B}_\perp$, no longer close as the particles go from passing to trapped and back. An analysis of the resulting transport leads to collisionless diffusion which scales as Eq. (4), and which is also proportional to $\sin^2\alpha$ (provided that $m < 3$),

$$D_r \sim \omega_E (\Delta r)^2 \frac{\Delta\phi}{T} \sin^2\alpha. \tag{6}$$

Stellarator symmetry can be seen to require $\alpha = 0$, in the following manner. Replicate the non-neutral plasma and external fields using an even periodic extension about the end of the plasma, and measure the origin of z from this point, and the origin of θ from θ_B. Then, the total electrostatic potential due to the squeeze potential plus the induced potential from the magnetic tilt will have a point-reflection symmetry about $z=0$ and $\theta = 0$: $\phi(r,-\theta,-z) = \phi(r,\theta,z)$ (stellarator symmetry[2]) *provided that* $\alpha = 0$. Furthermore, this symmetry is broken if $\alpha \neq 0$. Of course, the radial transport is unaffected by this periodic extension.

A summary of the different transport regimes is shown in Fig. 4, which sketches the radial diffusion coefficient versus collision frequency.

IV. TRANSPORT MEASUREMENTS

We now turn to a discussion of the experiments that have measured this radial superbanana transport in quiescent,

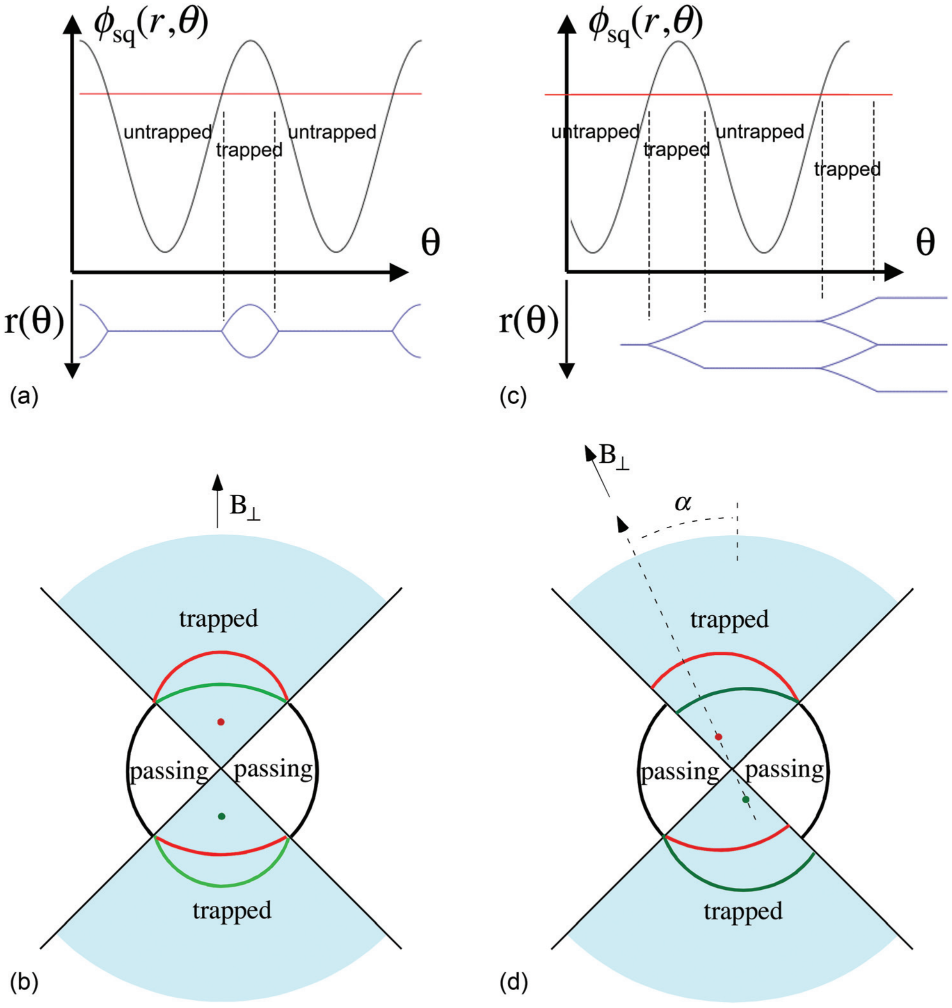

FIG. 3. (Color) (a) Separatrix potential $\phi_{sq}(r,\theta)$ and the orbits $r(\theta)$ for particles with given energy shown by the red line, for the symmetric case ($\alpha = 0$) when the ruffles are aligned with the magnetic tilt. Such particles transit from trapped to passing and back at the same radius. (b) End-on view of the orbits for the case of (a). The red orbits are trapped in the right well and are shifted circles centered on the red dot. The green orbits are trapped in the left well and are shifted circles centered on green dot. (c) Same as (a) but with broken stellarator symmetry, $\alpha \neq 0$. Now orbits no longer close radially and particles take random radial steps as they are randomly trapped in the left or right wells. (d) Same as (b) but for broken stellarator symmetry. Orbits are followed as they transit once from passing to trapped in either the left (green) or right (red) wells.

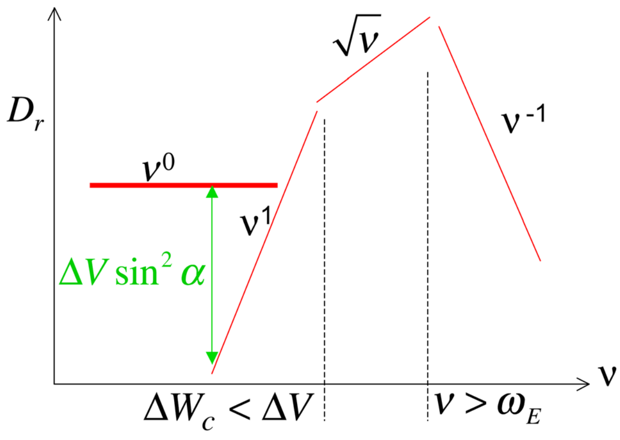

FIG. 4. (Color online) Schematic view of the different transport regimes.

low-collisionality pure electron plasmas.[10–12] Electrons are confined radially by a nominally uniform axial magnetic field $0.4 < B < 12$ kG and are confined axially by voltages $V_c = -100$ V on end cylinders of radius $R_w = 3.5$ cm. The electron columns have length $L_p = 49$ cm, and radial density profile $n(r)$ with central density $n_0 \approx 1.6 \times 10^7$ cm^{-3}, giving line density $N_L = \pi R_p^2 n_0 \approx 6.1 \times 10^7\,\text{cm}^{-1}$. The unneutralized charge results in an equilibrium potential energy $\Phi_e(r)$ with $\Phi_{e0} \approx +28$ eV at $r = 0$. This gives an $E \times B$ rotation frequency $f_E(r) = \omega_E/(2\pi)$ which decreases monotonically from $f_{E0} \approx 230\,\text{kHz} \times (B/1\text{kG})^{-1}$. The bulk electrons have a near-Maxwellian velocity distribution with thermal energy $T \lesssim 1$ eV, giving axial bounce frequency $f_b \lesssim$ 430 kHz, and electron-electron collision frequency $\nu \sim 200\,\text{s}^{-1}$.

The electrostatic trapping barrier $\phi_{\text{sq}}(r,\theta) = \phi_{s0}(r) + \Delta\phi_m(r)\cos[m(\theta - \theta_m)]$ is created by voltages applied to θ-sections of the central electrode. Here, we focus on $m = 2$ ruffles, created by voltages $\pm\Delta V_2$ applied to four 60° sectors, extending over $\Delta z = 3.8$ cm near the $z = 0$ center. At every radius, low energy particles are trapped in either the left or right end, whereas higher energy passing particles transit the entire length of the column. The characteristic separatrix energy is ruffled in θ by $\Delta\phi_m(r) \sim q\Delta V_m (r/R_w)^m$, further reduced inside the column by Debye shielding.

In the experiments, we diagnose the bulk expansion rate $\nu_{\langle r^2\rangle}$, defined as the rate of change of the plasma mean-square radius

$$\nu_{\langle r^2\rangle} \equiv \frac{1}{\langle r^2\rangle}\frac{d\langle r^2\rangle}{dt}, \tag{7}$$

where $\langle r^2\rangle \equiv 1/N \int d^3 r n(\mathbf{r},t) r^2$. Fortunately, $\nu_{\langle r^2\rangle}$ can be accurately and readily obtained by measuring the frequency $f_2(t)$ of a small amplitude $m_\theta = 2, k_z = 0$ diocotron mode, as $\nu_{\langle r^2\rangle} = -(1/f_2)(df_2/dt)$. This relation arises because $f_2 \propto \langle n\rangle$, and $\langle n\rangle \propto 1/\langle r^2\rangle$; and it has been verified by independent camera-dump measurements of $n(r,\theta,t)$. The bulk expansion rate $\nu_{\langle r^2\rangle}$ is an integral measure of the full radial flux that includes both mobility and diffusive contributions, both being proportional to the radial diffusion coefficient $D_r(r)$.[9,13]

An example of the expansion data obtained from this diagnostic is shown in Fig. 5. In Fig. 5(a), $\nu_{\langle r^2\rangle}$ is measured versus tilt direction θ_B, for various tilt magnitudes ϵ_B. The striking $\sin^2(\theta_B - \theta_2)$ dependence of the ruffle-induced transport makes the data unambiguous over a wide range of parameters. Figure 5(b) shows $\nu_{\langle r^2\rangle}$ versus ϵ_B, displaying the expected ϵ_B^2 dependence for small ϵ_B. We note, however, that scalings closer to $\epsilon_B^{1/2}$ are observed for ϵ_B only 2–3 times larger than displayed here. We compare this data, taken for various values of B, and ruffle strengths, to theory as described below.

A detailed analysis[6,9] of random transitions between equal trapping regions driven by rotation across $m = 2$ separatrix ruffles gives neoclassical asymmetric superbanana radial diffusion coefficient

$$D_r(r) = \frac{1}{4} F_M(\phi_{s0}) f_E \Delta r^2 \times \{\Delta W_c \hat{D}_c + \Delta\phi_2 \hat{D}_{\Delta\phi} \sin^2\alpha\}. \tag{8}$$

The (dimensionless) collisional bounce-averaged transport coefficient $\hat{D}_c$ and the (dimensionless) ruffle coefficient $\hat{D}_{\Delta\phi}$ are shown in Fig. 6 for $m = 2$, calculated in Ref. 9 as functions of the normalized ruffle strength $\Delta\phi/\Delta W_c$. While the ruffle-induced transport coefficient $\hat{D}_{\Delta\phi}$ is nearly independent of $\Delta\phi/\Delta W_c$, the collisional coefficient $\hat{D}_c$ shows a fast decline as chaotic particle transitions become dominant, and

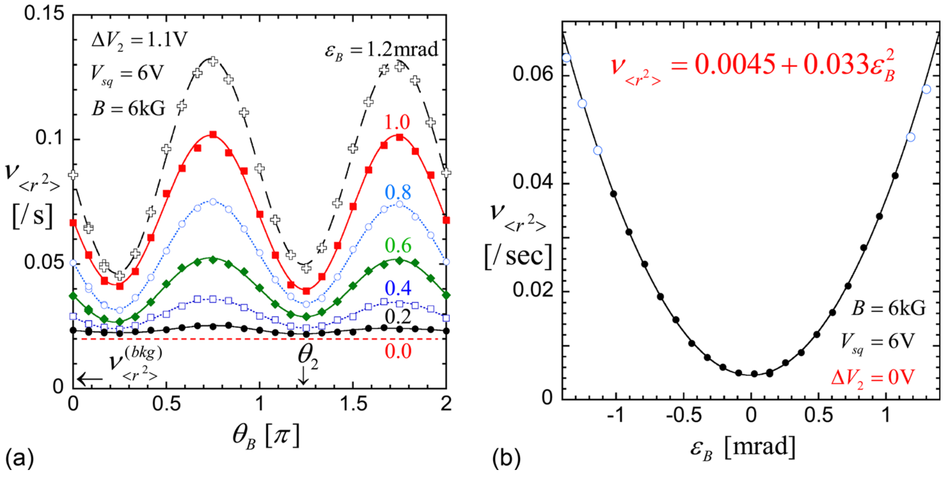

FIG. 5. (Color online) (a) Measured transport rates $\nu_{\langle r^2\rangle}$ versus tilt direction θ_B, for 6 tilt angles ϵ_B, showing the distinctive $\sin^2(\theta_B - \theta_2)$ signature of chaotic transport from the $m = 2$ ruffled separatrix. (b) Measured transport rates versus tilt angle ϵ_B with no applied ruffle with an ϵ_B^2 fit to the solid data points only, showing the expected ϵ_B^2 scaling of collisional neoclassical transport. The same ϵ_B^2 scaling is observed for ruffle-induced chaotic transport.

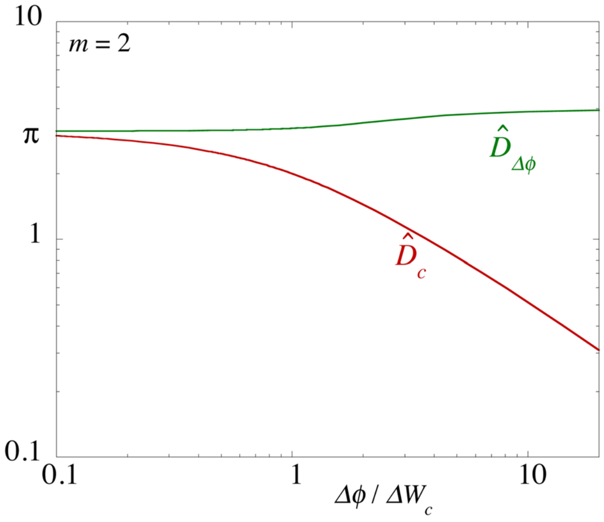

FIG. 6. (Color online) Predicted dimensionless diffusion coefficients $\hat{D}_c$ and $\hat{D}_{\Delta\phi}$ for collisional and chaotic transport, versus the ruffle magnitude $\Delta\phi$ scaled to the collisional separatrix layer width ΔW_c, for an $m = 2$ ruffle. Ruffles reduce D_c but cause large chaotic transport from $D_{\Delta\phi}$ unless the $\alpha = 0$ symmetry is perfect.

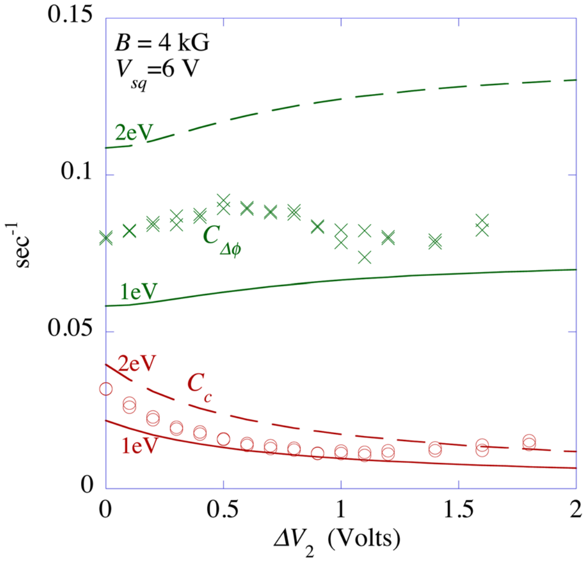

FIG. 7. (Color online) Comparison of theory (solid curves for a 1 eV plasma and dashed curves for a 2 eV plasma) and experiments (points) for the total radially averaged transport rates C_c and $C_{\Delta\phi}$ from collisional and chaotic transport, for one data set at $B = 4$ kG.

smooth out the discontinuity of F_M. In the case of aligned $m = 2$ ruffles ($\sin^2\alpha \approx 0$), this causes measurable suppression of collisional superbanana transport.

We obtain a prediction for the expansion rate by integrating the theoretical expression for the diffusion versus radius across the measured density profile in the given trap potentials

$$\nu_{\langle r^2\rangle} = C_c\left(\frac{\epsilon_B}{1\mathrm{mr}}\right)^2 + C_{\Delta\phi}\left(\frac{\epsilon_B}{1\mathrm{mr}}\right)^2\left(\frac{\Delta V_2}{1\mathrm{V}}\right)^2 \sin^2\alpha. \qquad (9)$$

The first term C_c is due to the collisional diffusion $\hat{D}_c$, and the second term $C_{\Delta\phi}$ is due to the chaotic $\hat{D}_{\Delta\phi}$ diffusion caused by separatrix ruffles. We note that evaluation of these coefficients requires knowledge of the plasma density and temperature as well as the error-field-induced potentials as a function of radius. These potentials are obtained by determining the self-consistent linear response of the plasma to the field errors, assuming collisionless bounce-averaged dynamics for the plasma. A more detailed discussion of this algorithm will be presented elsewhere. The theory is plotted for both 1 eV and 2 eV temperatures. The bulk temperature near $r = 0$ is measured to be roughly 1 eV, but the effective temperature at the radial edge, where most transport occurs, may be somewhat hotter.

This theory result is compared to the experiments by fitting the α and ϵ_B-dependence of the data to the dependences in the theory. For $\Delta\phi = 0$ (no ruffles), the expansion rate is roughly independent of α as expected from the theory, and the observed transport scales as ϵ_B^2, with a small offset due to background transport caused by small uncontrolled asymmetries. Performing similar fits for different values of $\Delta\phi$ and B leads one to experimentally determined values of the coefficients C_c and $C_{\Delta V}$ shown in Fig. 7 for $B = 4$ T. The collisional coefficient C_c shows a fall-off with increasing ruffle strength, as expected in the ν^1 regime for the symmetric case $\alpha = 0$. The chaotic coefficient $C_{\Delta\phi}$ is roughly independent of ruffle strength, also as expected theoretically. Theory shows fairly strong temperature dependence mainly because when T increases the induced asymmetry potential due to the magnetic tilt is less shielded and penetrates further into the plasma.

As the magnetic field is varied, the expansion coefficients also vary as expected theoretically, as shown in Fig. 8. For large magnetic fields, the collisional coefficient C_c for $\Delta\phi = 0$ scales as $1/B^{0.62}$, which is close to the $1/\sqrt{B}$ scaling expected for the $\sqrt{\nu}$ regime when there are no ruffles. The

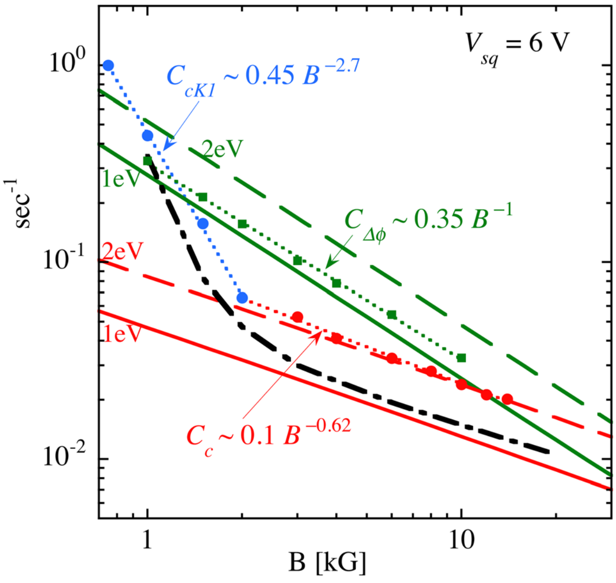

FIG. 8. (Color online) Comparison of theory (solid and dotted-dashed curves for a 1 eV plasma, and dashed curves for a 2 eV plasma) and experiments (points, dotted power-law fits), for the radially averaged transport rates from bounce-averaged collisional (C_c), bounce-averaged chaotic ($C_{\Delta\phi}$), and bounce-resonant collisional (C_{cK1}) neoclassical transport. The data and theory for C_c and C_{cK1} are for $\Delta V_2 = 0$, and for $C_{\Delta\phi}$ the data and theory are for $\Delta V_2 = 1$ V.

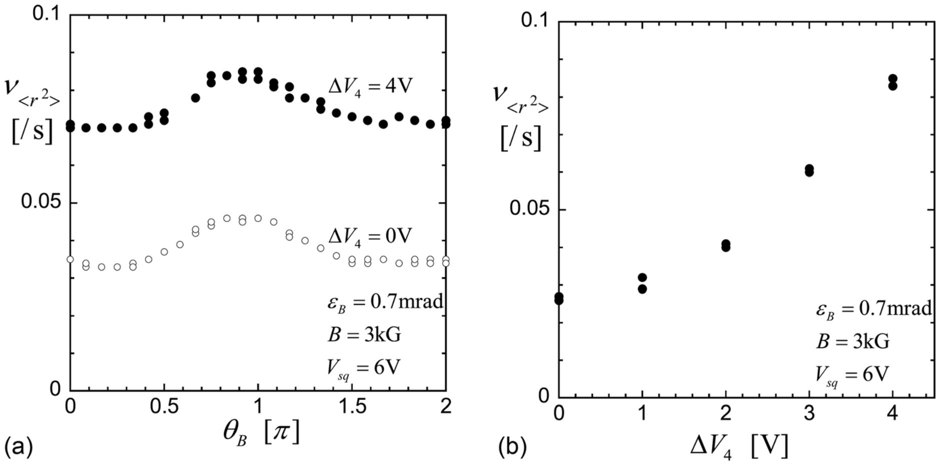

FIG. 9. (a) Measured transport $\nu_{\langle r^2\rangle}$ versus tilt direction θ_B, without and with $m = 4$ ruffle voltage ΔV_4. With ruffle, strong chaotic transport occurs at all symmetry angles. (b) Measured $\nu_{\langle r^2\rangle}$ versus ruffle strength ΔV_4, showing the decreasing collisional contribution and linearly increasing chaotic contribution as ΔV_4 increases.

chaotic coefficient $C_{\Delta\phi}$ scales as $1/B$, also as expected from the collisionless theory of Eq. (4). In this plot, the bounce-averaged theory for each coefficient is plotted as the solid and dashed lines, for 1 eV and 2 eV plasmas, respectively.

The 1 eV curve for C_c is a factor of $\sqrt{2}$ lower than a previously published theory curve[11,12] due to a factor of 2 error in the collision rate used previously. The corrected 1 eV curve shown in Fig. 8 has the same scaling with B as the data but is roughly a factor of 2 smaller than the measurements. One explanation for this discrepancy is the possibility that the plasma edge is at higher temperature, as shown by the 2 eV theory curve. Other possibilities also exist. For instance, it may be the case that the energy-dependent Fokker-Planck collision rate used in the theory,[7] which assumes a Maxwellian velocity distribution, underestimates the rate at which particles scatter across the separatrix. The source of the discrepancy will be the subject of further experimental and theoretical investigations.

V. BOUNCE-RESONANT TRANSPORT

There are also neoclassical fluxes[13,14] caused by collisions acting on bounce-rotation resonant orbits, and these have been neglected in the bounce-averaged theory presented above. These fluxes lead to extra "kinetic" terms in the expansion rate, which expand Eq. (9) to

$$\nu_{\langle r^2\rangle} = C_c\left(\frac{\epsilon_B}{1\text{mr}}\right)^2 + C_{\Delta V}\left(\frac{\epsilon_B}{1\text{mr}}\right)^2\left(\frac{\Delta V_2}{1\text{V}}\right)\sin^2\alpha + C_{cK1}\left(\frac{\epsilon_B}{1\text{mr}}\right)^2 + C_{cK2}\left(\frac{\Delta V_2}{1\text{V}}\right)^2. \quad (10)$$

The first two terms are the bounce-averaged terms as before, while the last two terms arise from bounce-rotation resonances in the controlled error fields of the magnetic tilt (C_{cK1}) and of the separatrix ruffles (C_{cK2}). Experimentally, the coefficient C_{cK2} can be extracted from the data due to its $(\Delta V_2)^2$ scaling. However, the coefficient C_{cK1} is distinguished from C_c by its substantially stronger B-dependence, and by its presence even without an applied V_{sq} barrier.

The two coefficients C_{cK1} and C_{cK2} can be calculated theoretically by separately solving for the neoclassical fluxes due to the magnetic tilt and the ruffled squeeze potential. We do this by determining the self-consistent error potential within the plasma due to a tilt and separately due to the ruffled squeeze, both in the collisionless bounce-averaged limit. We then use these linear error potentials to determine perturbed distribution functions as the solution to the linearized Boltzmann equation with Fokker-Planck collisions. Each perturbed distribution function then yields a radial transport coefficient, obtained by integrating the distribution function over the perturbed potential as described in Ref. 13. The resulting transport coefficient C_{cK1} is plotted as the dotted-dashed line in Fig. 8 versus magnetic field for the case of a magnetic tilt without separatrix ruffles, and agrees reasonably well with the observed magnetic scaling both at small and large magnetic fields. Preliminary work on C_{cK2} also shows a similar agreement, although the data have not been fully analyzed yet.

VI. CHAOTIC TRANSPORT FOR HIGHER RUFFLE MODE NUMBER

Significantly, theory[9] and experiments show that strong chaotic transport may persist even with "stellarator symmetry." For example, Fig. 9(a) shows chaotic transport with *no* dependence on $\alpha \equiv \theta_B - \theta_4$, from a $\Delta V_4 \cos 4(\theta - \theta_4)$ ruffle. With $\Delta V_4 = 0$, the lower points show collisional neoclassical transport, with apparent weak θ_B-dependence due to imperfect alignment of $\mathbf{B}$. Application of a $m = 4$ ruffle with $\Delta V_4 = 1$ V causes strong chaotic transport which is also essentially independent of α. Both the collisional and chaotic components scale as ϵ_B^2. In Fig. 9(b), measurements of $\nu_{\langle r^2\rangle}$ versus ΔV_4 exhibit a collisional component which decreases with ΔV_4, and a chaotic component proportional to ΔV_4. This is analogous to the $m = 2$ ruffle theory and experiments, but for $m = 4$ there is no $\sin^2\alpha$ dependence. More broadly, theory and experiments both demonstrate that there is no favored symmetric configuration where transport is reduced by any ruffle with $m \geq 3$.

ACKNOWLEDGMENTS

This work was supported by National Science Foundation Grant No. PHY-0903877 and Department of Energy Grant No. DE-SC0002451.

[1] H. Mynick, Phys. Plasmas **13**, 058102 (2006).
[2] R. L. Dewar and S. R. Hudson, Physica D **112**, 275 (1998).
[3] J. W. Connor and R. J. Hastie, Phys. Fluids **17**, 114 (1974).
[4] M. N. Rosenbluth, D. W. Ross, and D. P. Kostamorov, Nucl. Fusion **12**, 3 (1972).
[5] A. A. Galeev, R. Z. Sagdeev, H. P. Furth, and M. N. Rosenbluth, Phys. Rev. Lett. **22**, 511 (1969).
[6] D. H. E. Dubin, C. F. Driscoll, and Y. A. Tsidulko, Phys. Rev. Lett. **105**, 185003 (2010).
[7] T. J. Hilsabeck and T. M. O'Neil, Phys. Plasmas **10**, 3492 (2003).
[8] H. Mynick, Phys. Fluids **26**, 2609 (1983).
[9] D. H. E. Dubin and Y. Tsidulko, Phys. Plasmas **18**, 062114 (2011).
[10] A. A. Kabantsev and C. F. Driscoll, Phys. Rev. Lett. **89**, 245001 (2002).
[11] A. A. Kabantsev, D. H. E. Dubin, C. F. Driscoll, and Yu. A. Tsidulko, Phys. Rev. Lett. **105**, 205001 (2010).
[12] A. A. Kabantsev and C. F. Driscoll, Prob. At. Sci. Technol. **6**, 26 (2010).
[13] D. H. E. Dubin, Phys. Plasmas **15**, 072112 (2008).
[14] F. L. Hinton and R. D. Hazeltine, Rev. Mod. Phys. **48**, 239 (1976).